Journal of Sound and Vibration (2000) **233**(4), 557–571
doi:10.1006/jsvi.1999.2813, available online at http://www.idealibrary.com on IDEAL®

ANALYSIS OF NON-LINEAR DYNAMICS AND BIFURCATIONS OF A SHALLOW ARCH SUBJECTED TO PERIODIC EXCITATION WITH INTERNAL RESONANCE

Q. Bi

Department of Mechanics, Tianjin University Tianjin, 300072, *The People's Republic of China*

AND

H. H. Dai

Department of Mathematics, City University of Hong Kong, Hong Kong

(*Received* 29 *April* 1997, *and in final form* 25 *June* 1999)

In this paper, the dynamical behavior of a shallow arch subjected to periodic excitation with internal resonance is explored in detail. The parametric plane is then divided into different types of regions by the transition boundaries according to the types of the steady state solutions. A time-integration scheme is used to find the numerical solutions in these regions, which agree with the analytic results. Finally, numerical simulation is also applied to obtain double-period cascading bifurcations leading to chaos and the steady state period-3 solution is shown in the chaos region in the end.

1. INTRODUCTION

A lot of results on the dynamics of the first order mode of the shallow arch subjected to periodic excitation have been presented (e.g., see references [1, 2]). However, it has been noticed that when the shallow arch possesses suitable initial static deflection, internal resonance may arise in the system. Internal resonance has been found in many physical problems. The non-linear response of a circular pipe conveying fluid [3], the stretched string dynamics [4, 5] and the double pendulum [6] are examples of some of the recent studies. When the internal resonance occurs, the two modes may react with each other and energy may be transferred between the two resonant modes. It is needed to study the two modes simultaneously in order to obtain the dynamical behavior of the system. Tien *et al.* [7, 8] examined the local and global bifurcation of the shallow arch in the presence of 1 : 1 and 1 : 2 internal resonance by using the method developed by Kovacic and Wiggins [9]. In this paper, the investigation, combined with the results presented in our previous paper [6] is extended to study dynamical behaviors and bifurcations of the system. Transition boundaries have been obtained such that the parametric plane can be divided into different types of regions according to the types of the solutions. Numerical approach is employed to find the solutions in these regions, which agree with the analytic results. The route to chaos by period-doubling bifurcations as well as the period-3 solution in the chaos region is simulated in the end.

2. PROBLEM STATEMENT

We consider the shallow arch shown in Figure 1. Assume that the arch possesses initial static deflection, $\bar{w}(x, t)$, before the loading of the transverse periodic force $p(x, t)$. The

0022-460X/00/240557 + 15 $35.00/0

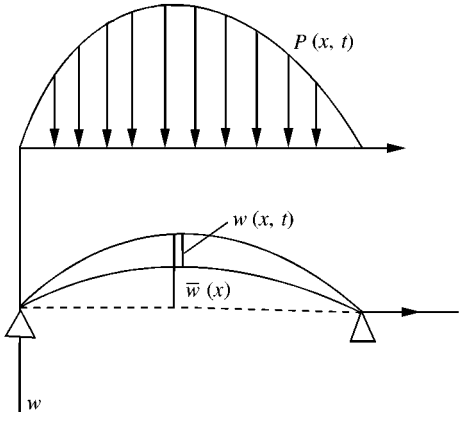

Figure 1. Model.

dynamical deflection, $w(x, t)$, occurs when the periodic excitation is applied to the system. The dimensionless equations of motion can then be given in the form [6, 7]

$$\ddot{q}_1 + \beta_1\dot{q}_1 + (1 + 2q_0^2)q_1 - 3q_0q_1^2 - 4q_0q_2^2 + q_1^3 + 4q_1q_2^2 - \lambda_0 + \rho\cos(\gamma t) = 0, \quad (1a)$$

$$\ddot{q}_2 + \beta_2\dot{q}_2 + 16q_2 + 4q_2(q_1^2 + 4q_2^2 - 2q_0q_1) = 0, \quad (1b)$$

where q_0 is the amplitude of initial static deflection, q_1, q_2 express the amplitudes of the first order mode and the second order mode, respectively, λ_0 is the loading parameter of the static deflection, and ρ, γ are the amplitude and the frequency of the periodic force respectively. Defining $Q_1 = q_1 - q_0$, $Q_2 = q_2$, when $\rho = 0$, the equilibrium points may be written in the following form:

$$Q_{10}^3 - Q_{10}(q_0^2 - 1) = \lambda_0 - q_0, \quad Q_{20} = 0. \quad (2)$$

For convenience, we redefine q_1, q_2. Let

$$Q_1 = Q_{10} + \varepsilon q_1, \qquad Q_2 = Q_{20} + \varepsilon q_2,$$

$$\beta_1 = \varepsilon\delta_1, \qquad \beta_2 = \varepsilon\delta_2, \qquad \rho = \varepsilon^2\mu, \quad (\varepsilon \ll 1). \quad (3)$$

Substituting equations (2), (3) into equations (1a, b) results in

$$\ddot{q}_1 + \omega_1^2 q_1 + \varepsilon[\delta_1\dot{q}_1 + 3Q_{10}q_1^2 + 4Q_{10}q_2^2 + \mu\cos(\gamma t)] + \varepsilon^2(q_1^3 + 4q_1q_2^2) = 0, \quad (4a)$$

$$\ddot{q}_2 + \omega_2^2 q_2 + \varepsilon(\delta_2\dot{q}_2 + 8Q_{10}q_1q_2) + \varepsilon^2(16q_2^3 + 4q_1^2q_1) = 0, \quad (4b)$$

where $\omega_1^2 = 3Q_{10} + (1 - q_0^2)$, $\omega_2^2 = 4[Q_{10}^2 + (4 - q_0^2)]$. It is easy to find that if the parameters are taken at the solid line in Figure 2, then $\omega_1 = 2\omega_2$, which means that 1 : 2 internal resonance takes place.

3. STEADY STATE SOLUTIONS

We now apply the following canonical change of variables to equations (4a, b):

$$q_i = \sqrt{2a_i}\cos(\omega_i t + \theta_i), \qquad p_i = -\omega_i\sqrt{2a_i}\sin(\omega_i t + \theta_i), \quad i = 1, 2, \quad (5)$$

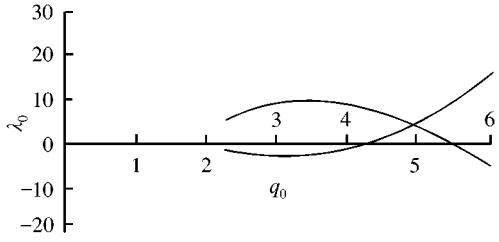

Figure 2. Condition of 1 : 2 internal resonance.

where $p_1 = \dot{q}_1, p_2 = \dot{q}_2$. In order to investigate the dynamics in the presence of both external and 1 : 2 internal resonance, we introduce the detuning parameters σ_1 and σ_2 such that

$$\omega_1^2 = \gamma^2 - \varepsilon\sigma_1, \qquad \omega_2^2 = \gamma^2 - \varepsilon\sigma_2, \tag{6}$$

where σ_1 and σ_2 represent the deviation of the excitation frequency from the first and second natural frequencies respectively. By using the average method, one may obtain the following averaged system [7]:

$$\dot{a}_1 = \varepsilon\left[-\delta_1 a_1 + \frac{2Q_{10}\sqrt{2a_1}a_2}{\gamma}\sin(\theta_1 - 2\theta_2) + \mu\frac{\sqrt{2a_1}}{2\gamma}\sin\theta_1\right],$$

$$a_1\dot{\theta}_1 = \varepsilon\left[-\frac{\sigma_1}{\gamma}a_1 + \frac{Q_{10}\sqrt{2a_1}a_2}{\gamma}\cos(\theta_1 - 2\theta_2) + \mu\frac{\sqrt{2a_1}}{4\gamma}\cos\theta_1\right],$$

$$\dot{a}_2 = \varepsilon\left[-\delta_2 a_2 - \frac{8Q_{10}\sqrt{2a_1}a_2}{\gamma}\sin(\theta_1 - 2\theta_2)\right],$$

$$a_2\dot{\theta}_2 = \varepsilon\left[-\frac{\sigma_2}{\gamma}a_2 + \frac{4Q_{10}\sqrt{2a_1}a_2}{\gamma}\cos(\theta_1 - 2\theta_2)\right]. \tag{7}$$

Using the canonical change of variables

$$u_i = \sqrt{2a_i}\cos(\theta_i), \qquad v_i = -\sqrt{2a_i}\sin(\theta_i) \quad (i = 1, 2) \tag{8}$$

in equations (7), we obtain

$$\dot{u}_1 = \varepsilon\left[-\frac{\delta_1}{2}u_1 - \frac{\sigma_1}{\gamma}v_1 + \frac{2Q_{10}}{\gamma}u_2 v_2\right],$$

$$\dot{v}_1 = \varepsilon\left[\frac{\sigma_1}{\gamma}u_1 - \frac{\delta_1}{2}v_1 - \frac{\mu}{2\gamma} - \frac{Q_{10}}{\gamma}(u_2^2 - v_2^2)\right],$$

TABLE 1

Number of the solution a_2

Λ_0	$F \geqslant 0$	Number of the solution a_2	Solutions of a_2
$\Lambda_0 > 0$	$\Lambda_0 \geqslant F$	2	$\Lambda_0 \pm \sqrt{F}$
	$\Lambda_0 < F$	1	$\Lambda_0 + \sqrt{F}$
$\Lambda_0 \leqslant 0$	$\lvert\Lambda_0\rvert \leqslant F$	1	$\Lambda_0 + \sqrt{F}$
	$\lvert\Lambda_0\rvert > F$	0	

$$\dot{u}_2 = \varepsilon\left[-\frac{\delta_2}{2}u_2 - \frac{\sigma_2}{\gamma}v_2 + \frac{4Q_{10}}{\gamma}(u_2v_1 - u_1v_2)\right],$$

$$\dot{v}_2 = \varepsilon\left[\frac{\sigma_2}{\gamma}u_2 - \frac{\delta_2}{2}v_2 - \frac{4Q_{10}}{\gamma}(u_1u_2 + v_1v_2)\right]. \tag{9}$$

From equations (7), one may obtain the following two types of solutions:

(1) *Single-mode steady state solutions* ($a_1 \neq 0, a_2 = 0$):

$$a_1 = \frac{\mu^2}{2(\delta_1^2\gamma^2 + 4\sigma_1^2)}, \qquad tg\theta_1 = \frac{\delta_1\gamma}{2\sigma_1}. \tag{10}$$

(2) *Coupled-mode steady state solutions*:

$$a_1 = \frac{\delta_2^2\gamma^2 + 4\sigma_2^2}{128Q_{10}^2}, \qquad a_2 = a_2^{\pm} = \frac{[(\sigma_1\sigma_2/\gamma^2 - \delta_1\delta_2/4) \pm \sqrt{F}]}{8Q_{10}^2}, \tag{11}$$

where $F = (4Q_{10}^2\mu^2/\gamma^4) - [(\delta_1\delta_2 + \sigma_1\sigma_2)/2\gamma]^2$. It is obvious to see that non-trivial solution a_2 exists only when $F \geqslant 0$. Letting $\Lambda_0 = (\sigma_1\sigma_2/\gamma^2 - \delta_1\delta_2/4)$, the number of the solution a_2 is given in Table 1.

The stability of the solutions can be determined from equation (9). Letting $p = (u_1, v_1, u_2, v_2)^{\mathrm{T}}$ and $p_0 = (u_{10}, v_{10}, u_{20}, v_{20})^{\mathrm{T}}$, where p_0 is the steady state solution, from equation (9), one may obtain

$$\dot{p} = H(p). \tag{12}$$

Introduce the following perturbation

$$p = p_0 + q, \tag{13}$$

where p_0 is the steady state solution of equation (9), i.e., $H(p_0) = 0$. Substituting equation (13) into equation (12) results in the following first order approximation:

$$\dot{q} = \left[\frac{\partial H}{\partial p}\right]_{p=p_0} \quad q = Jq, \tag{14}$$

where

$$J = [F_{ij}] = \left[\frac{\partial H}{\partial P}\right]_{p=p_0}$$

$$= \begin{bmatrix} -\frac{\delta_1}{2} & -\frac{\sigma_1}{\gamma} & \frac{2Q_{10}}{\gamma} v_{20} & \frac{2Q_{10}}{\gamma} u_{20} \\ \frac{\sigma_1}{\gamma} & -\frac{\delta_1}{2} & -\frac{2Q_{10}}{\gamma} u_{20} & \frac{2Q_{10}}{\gamma} v_{20} \\ -\frac{4Q_{10}}{\gamma} v_{20} & \frac{4Q_{10}}{\gamma} u_{20} & -\frac{\delta_2}{2} + \frac{4Q_{10}}{\gamma} v_{10} & -\frac{\sigma_2}{\gamma} - \frac{4Q_{10}}{\gamma} u_{10} \\ -\frac{4Q_{10}}{\gamma} u_{20} & -\frac{4Q_{10}}{\gamma} v_{20} & \frac{\sigma_2}{\gamma} - \frac{4Q_{10}}{\gamma} u_{10} & -\frac{\delta_2}{2} - \frac{4Q_{10}}{\gamma} v_{10} \end{bmatrix}.$$

If all the eigenvalues of the Jacobian matrix J have negative real parts, the solution $p_0 = (u_{10}, v_{10}, u_{20}, v_{20})^{\mathrm{T}}$ is stable. We denote

$$\det(J - \lambda I) = \lambda^4 + A_3\lambda^3 + A_2\lambda^2 + A_1\lambda + A_0 = 0. \tag{15}$$

By the Routh–Hurwitz rule, from equation (15), one may find, when

$$A_0 = \det(J) > 0, \qquad A_1 > 0, \qquad A_2 > 0, \qquad A_3 > 0, \qquad A_1A_2A_3 - (A_0A_3^2 + A_1^2) > 0 \tag{16}$$

that all the values of λ in equation (15) have negative real parts, and the solution is stable. However, when

$$A_0 = \det(J) = 0, \qquad A_1 > 0, \qquad A_2 > 0, \qquad A_3 > 0, \qquad A_1A_2A_3 - A_1^2 > 0 \tag{17}$$

there is a simple zero eigenvalue. The solution may lose its stability and undergo a simple bifurcation. When

$$A_0 = \det(J) > 0, \qquad A_1 > 0, \qquad A_3 > 0, \qquad A_1A_2A_3 - (A_0A_3^2 + A_1^2) = 0, \tag{18}$$

there will be a pair of pure imaginary eigenvalues and the possible Hopf bifurcation will take place.

For the single-mode steady state solutions ($a_1 \neq 0, a_2 = 0$), the eigenvalues satisfy the following equations:

$$\begin{aligned} \lambda_{1,2}^2 + \delta_1\lambda_{1,2} + \left[\left(\frac{\delta_1}{2}\right)^2 + \left(\frac{\sigma_1}{\gamma}\right)^2\right] = 0, \\ \lambda_{3,4}^2 + \delta_1\lambda_{3,4} + \left[\left(\frac{\delta_2}{2}\right)^2 + \left(\frac{\sigma_2}{\gamma}\right)^2 - \frac{32a_1Q_{10}}{\gamma^2}\right] = 0. \end{aligned} \tag{19}$$

Since $\delta_1 > 0$, $\delta_2 > 0$, both of $\lambda_{1,2}$ have negative real parts. Therefore, if the condition

$$\left(\frac{\delta_2}{2}\right)^2 + \left(\frac{\sigma_2}{\gamma}\right)^2 - \frac{32a_1Q_{10}}{\gamma^2} > 0. \tag{20}$$

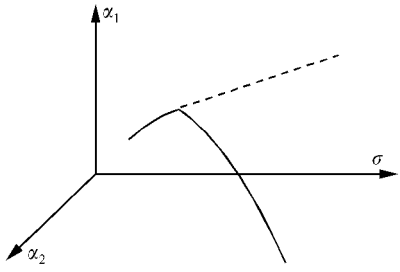

Figure 3. Single-mode motion leads to coupled-mode motion.

is satisfied, then the single-mode motion is stable. The critical line which defines the stability boundary of the single-mode motion can then be defined as

$$\left(\frac{\delta_2}{2}\right)^2 + \left(\frac{\sigma_2}{\gamma}\right)^2 - \frac{32a_1Q_{10}}{\gamma^2} = 0, \tag{21}$$

from which the coupled-mode motion described by equation (11) bifurcates from the single-mode motion (10), as shown in Figure 3. The energy of the system is transmitted from the first order mode to the second order mode.

For the coupled-mode steady state solutions ($a_1 \neq 0$, $a_2 \neq 0$), the characteristic equation can be expressed in the following form:

$$\det(J - \lambda I) = \lambda^4 + A_3\lambda^3 + A_2\lambda^2 + A_1\lambda + A_0 = 0, \tag{22}$$

where

$$\begin{aligned}
A_3 &= \delta_1 + \delta_2,\\
A_2 &= \delta_1\delta_2 + \frac{\delta_1^2}{4} + \frac{\sigma_1^2}{\gamma^2} + \frac{32a_1Q_{10}^2}{\gamma^2},\\
A_1 &= \frac{1}{4}\delta_1^2\delta_2 + \frac{\sigma_1^2\delta_2}{\gamma^2} + \frac{16a_2Q_{10}^2}{\gamma^2}(\delta_1 + \delta_2),\\
A_0 &= a_2\left[\frac{256Q_{10}^4}{\gamma^4}a_2 + \frac{32Q_{10}^2}{\gamma^2}\left(\frac{\delta_1\delta_2}{4} - \frac{\sigma_1\sigma_2}{\gamma^2}\right)\right].
\end{aligned} \tag{23}$$

Since $a_1 > 0$, $a_2 > 0$ (they represent the amplitudes of the first order mode and the second order mode respectively). It is easy to find that $A_1 > 0$, $A_2 > 0$, $A_3 > 0$. Therefore, the stable region for the coupled mode motion can be given in the following form:

$$A_0 = a_2\left[\frac{256Q_{10}^4}{\gamma^4}a_2 + \frac{32Q_{10}^2}{\gamma^2}\left(\frac{\delta_1\delta_2}{4} - \frac{\sigma_1\sigma_2}{\gamma^2}\right)\right] > 0, \qquad A_1A_2A_3 - (A_0A_3^2 + A_1^2) > 0 \tag{24}$$

which, in turn, gives two critical lines. One of these is described by

$$A_0 = a_2\left[\frac{256Q_{10}^4}{\gamma^4}a_2 + \frac{32Q_{10}^2}{\gamma^2}\left(\frac{\delta_1\delta_2}{4} - \frac{\sigma_1\sigma_2}{\gamma^2}\right)\right] = 0 \tag{25}$$

from which saddle-node bifurcation occurs. The second critical line is

$$A_1A_2A_3 - A_1^2 = 0 \tag{26}$$

which leads to a family of limit cycles bifurcating from the coupled-mode motion.

The physical parametric plane is divided into different regions by these bifurcation transition boundaries expressed by equations (21), (25) and (26). The solutions in these regions are different from each other. In the region of the Hopf bifurcation solution bounded by equation (26), there are very rich dynamical behaviors. Since the analytical method cannot solve the problems, we now turn to the numerical simulation in the following analysis.

4. NUMERICAL ANALYSIS

A numerical method is employed in this section in order to express the transition boundaries described in the above section to show how the solutions change with the parameters. Parts of the parameters are fixed at $\delta_1 = \delta_2 = 0{\cdot}1$, $Q_{10} = -\sqrt{24}$, $\mu = 0{\cdot}8$, $\gamma = \sqrt{48}$. The two detuning parameters σ_1 and σ_2 are chosen as the varying parameters to see how they influence the solutions. The transition boundaries on the parametric plane $(\sigma_1{-}\sigma_2)$ are given in Figure 4.

The plane of $(\sigma_1{-}\sigma_2)$ is divided by these transition boundaries into eight regions denoted by ①, ②, ③, ③′, ③″, ③‴, ④, ⑤.

In regions ①, ②, ③, ③′, there is only single-mode motion, i.e., $a_1 \neq 0$, $a_2 = 0$, and the single-mode motion is stable.

In regions ③″, ③‴, the single-mode motion loses its stability and a simple bifurcation occurs, which leads to coupled-mode motion, i.e., $a_1 \neq 0$, $a_2 \neq 0$. a_1 is stable, while a_2 has two branches, i.e., $a_2 = a_2^{\pm}$, where a_2^+ is stable and a_2^- is unstable.

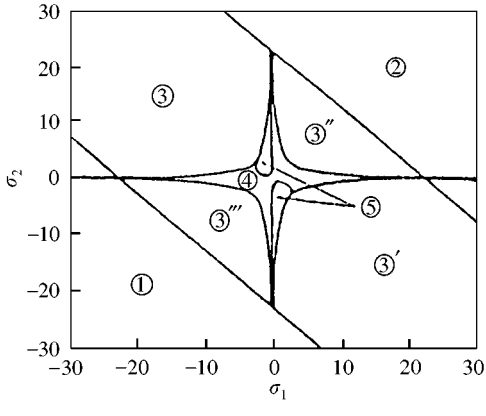

Figure 4. Transition boundaries on the plane $(\sigma_1{-}\sigma_2)$.

In region ④, the single-mode motion loses its stability and leads to coupled-mode motion by simple bifurcation. It is easy to find that the coupled-mode motion is stable by a simple eigenvalue analysis.

At the boundary of region ⑤, the coupled-mode motion loses its stability and leads to modulated motion by Hopf bifurcation. A family of limit cycles takes place at the transition boundary. The Hopf bifurcation leads to chaos by a set of period-doubling bifurcations, which we will show in the following text.

The pitchfork bifurcation occurs at the critical boundaries from ③, ③′, ③″, ③‴ to ④, and the saddle-node bifurcation takes place at the boundary from ③″ to ② and from ③‴ to ①, while the Hopf bifurcation starts at the transition boundary from ④ to ⑤.

The curves of $\sqrt{2a_1}$ and $\sqrt{2a_2}$ depending on the detuning parameter σ_1 and the bifurcation points are given in Figure 5 when $\sigma_2 = 2{\cdot}4$. When $\sigma_1 < -3{\cdot}15$, the single-mode motion $a_1 \neq 0$, $a_2 = 0$ is stable. When $\sigma_1 = -3{\cdot}15$, the pitchfork bifurcation occurs and the single-mode motion leads to stable coupled-mode motion. An interesting phenomenon called saturation is found, which means that a_1 does not change with the detuning parameter σ_1. When σ_1 increases to $-2{\cdot}74$, the coupled-mode motion $a_1 \neq 0$, $a_2 \neq 0$ loses its stability and the supercritical Hopf bifurcation takes place. When σ_1 increases to $-0{\cdot}05$, the subcritical Hopf bifurcation is found and the coupled-mode motion regains its stability. The saturation phenomenon is still observed. When σ_1 increases to 3·15, the pitchfork bifurcation occurs and the unstable solution $a_2 \neq 0$ is found. The saturation phenomenon disappears. When σ_1 further increases to 20·43, the saddle-node bifurcation takes place, which leads to the instability of the coupled-mode motion and the single-mode motion regains its stability.

The curves of $\sqrt{2a_1}$ and $\sqrt{2a_2}$ depending on the detuning parameter σ_2 and the bifurcation points are given in Figure 6 when $\sigma_1 = -2{\cdot}4$. When $\sigma_2 < -20{\cdot}43$, the single-mode motion is stable. At the point $\sigma_2 = -20{\cdot}43$, the saddle-node bifurcation is found and the single-mode motion leads to coupled-mode motion. There are two branches of $a_2 = a_2^{\pm}$, where the upper branch $a_2 = a_2^{+}$ is stable while the lower branch $a_2 = a_2^{-}$ is unstable. When σ_2 increases to $-3{\cdot}15$, the pitchfork bifurcation leads to the disappearance

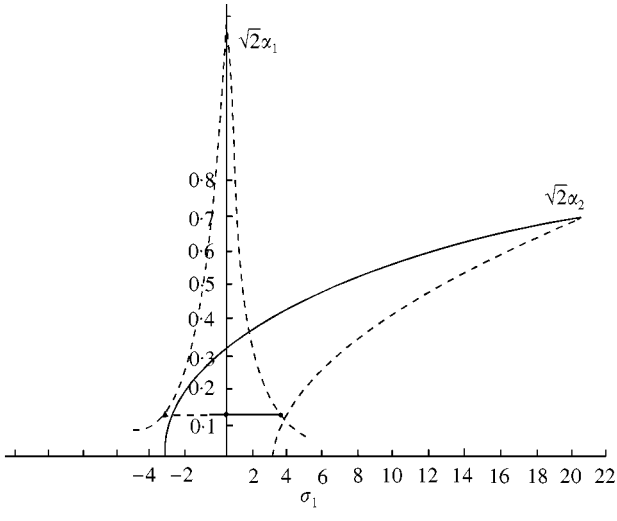

Figure 5. Response curves when $\sigma_2 = 2{\cdot}4$. – – –, unstable solution; ——, stable solution; ●, Pitchfork bifurcation; ◆, Hopf bifurcation; ▲, saddle-node bifurcation.

of $a_2 = a_2^-$. When σ_2 increases to 1·72, the coupled-mode motion loses its stability by supercritical Hopf bifurcation and the modulated motion is found. The coupled-mode motion regains its stability at the point $\sigma_2 = 3{\cdot}05$ by the supercritical Hopf bifurcation. The coupled-mode motion leads to the single-mode motion when σ_2 increases to 3·25.

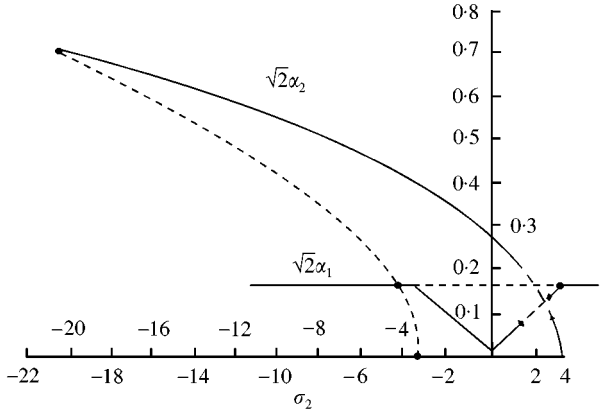

Figure 6. Response curves when $\sigma_1 = -2{\cdot}4$. – – –, unstable solution; ——, stable solution; ●, Pitchfork bifurcation; ◆, Hopf bifurcation; ▲, saddle-node bifurcation.

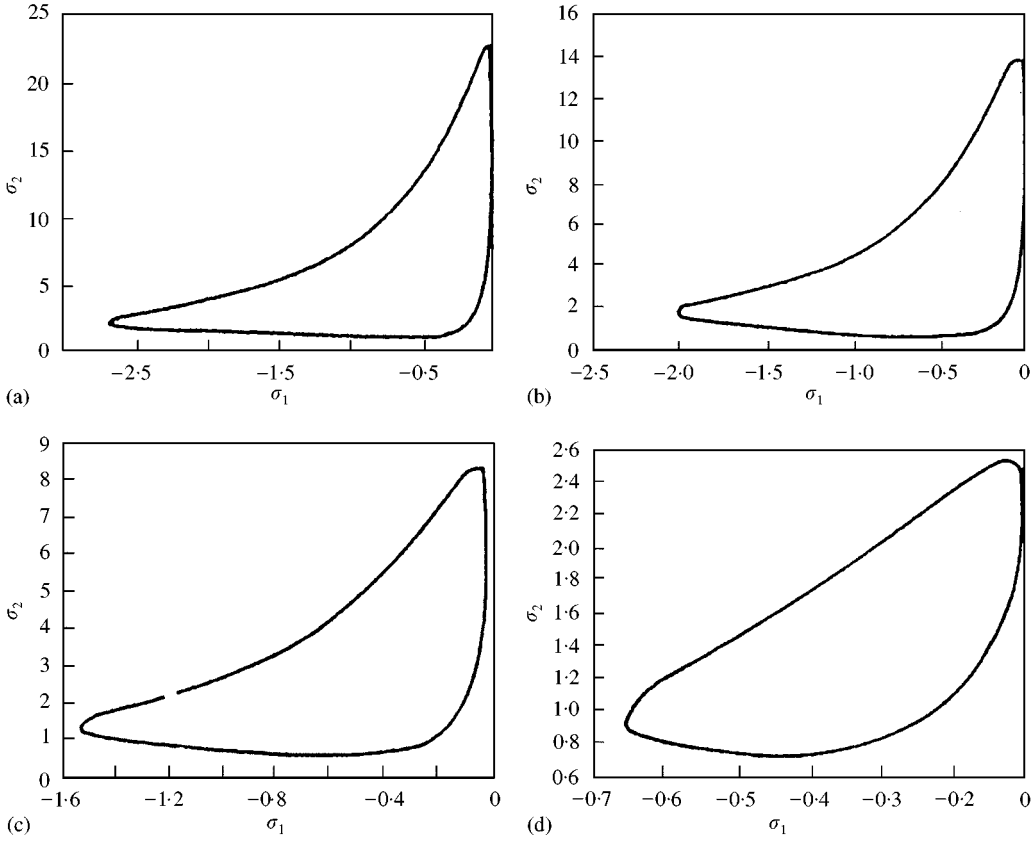

Figure 7. Transition boundaries of Hopf bifurcation. (a) $\mu = 0{\cdot}8$, (b) $\mu = 0{\cdot}5$, (c) $\mu = 0{\cdot}3$, (d) $\mu = 0{\cdot}1$.

The critical boundaries of Hopf bifurcation on the plane $(\sigma_1-\sigma_2)$ are given in Figure 7 when $\sigma_1 < 0$, $\sigma_2 > 0$, where $\mu = 0{\cdot}8, 0{\cdot}5, 0{\cdot}3, 0{\cdot}1$ respectively. It is noted that another set of critical boundaries of Hopf bifurcation which are symmetric to these boundaries about the axes (σ_1, σ_2) exist in the region $\sigma_1 > 0$, $\sigma_2 < 0$. We omit these symmetric boundaries for simplicity (see Figure 4 for reference).

It can be seen that with the decrease of the amplitude of external force μ, the regions for the Hopf bifurcation contract. The modulated motion which occurs at the Hopf bifurcation boundaries leads to complicated dynamical phenomena with the change of σ_1, σ_2.

In order to investigate the complicated dynamics in region ⑤ with the change of σ_1, σ_2, we fix some of the parameters with 1:2 internal resonance at $\delta_1 = \delta_2 = 0{\cdot}1$, $\mu = 0{\cdot}8$, $\gamma = \sqrt{48}$, $Q_{10} = -\sqrt{24}$, $\sigma_2 = 3{\cdot}04$. A time-integration scheme has been employed to find

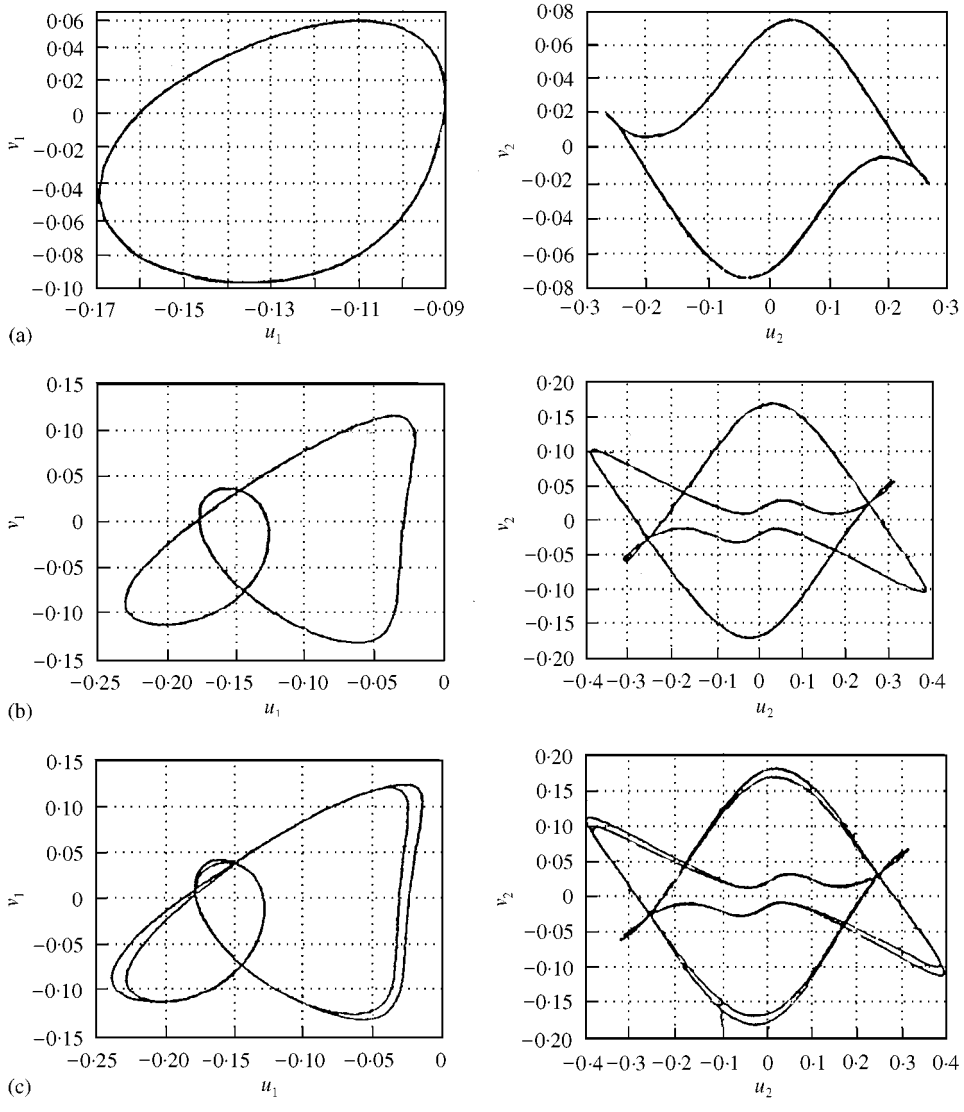

Figure 8. Period-doubling to chaos. (a) Period-1, (b) period-2, (c) period-4, (d) period-8, (e) chaos.

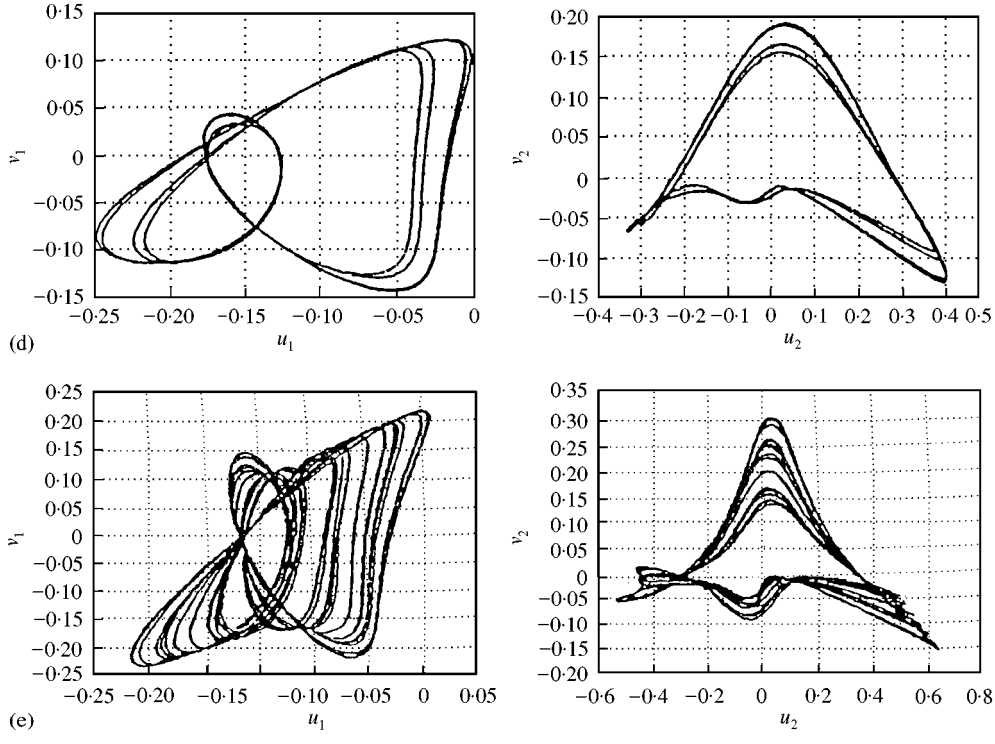

Figure 8. Continued.

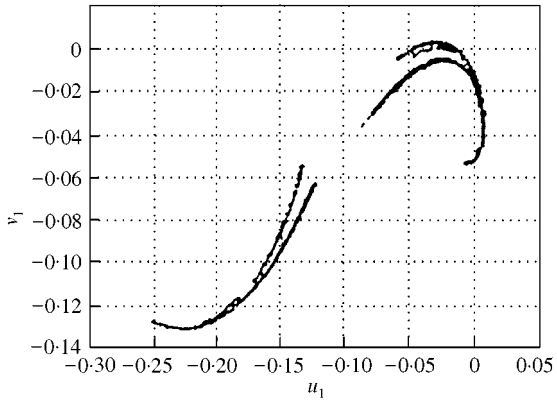

Figure 9. Poincare map on the plane $u_2 = 0$.

double-periodic motions leading to chaos—a well-known chaos scenario. The cascading bifurcation happens when σ_1 is increased from $-2{\cdot}0$. The sequence of period-doubling bifurcations is shown in Figures 8(a–e) where the detuning parameter is taken at $\sigma_1 = -2{\cdot}0$, $-1{\cdot}8$, $-1{\cdot}69$, $-1{\cdot}66$, $-1{\cdot}64$ respectively. The Poincare map which may be called strange attractor at the cross-section $u_2 = 0$ is shown in Figure 9 when $\sigma_1 = -1{\cdot}55$.

When σ_1 is increased to $-1{\cdot}48$, there exists a stable steady state solution of period-1 in the chaos region. This solution also leads to chaos by a sequence of period-doubling

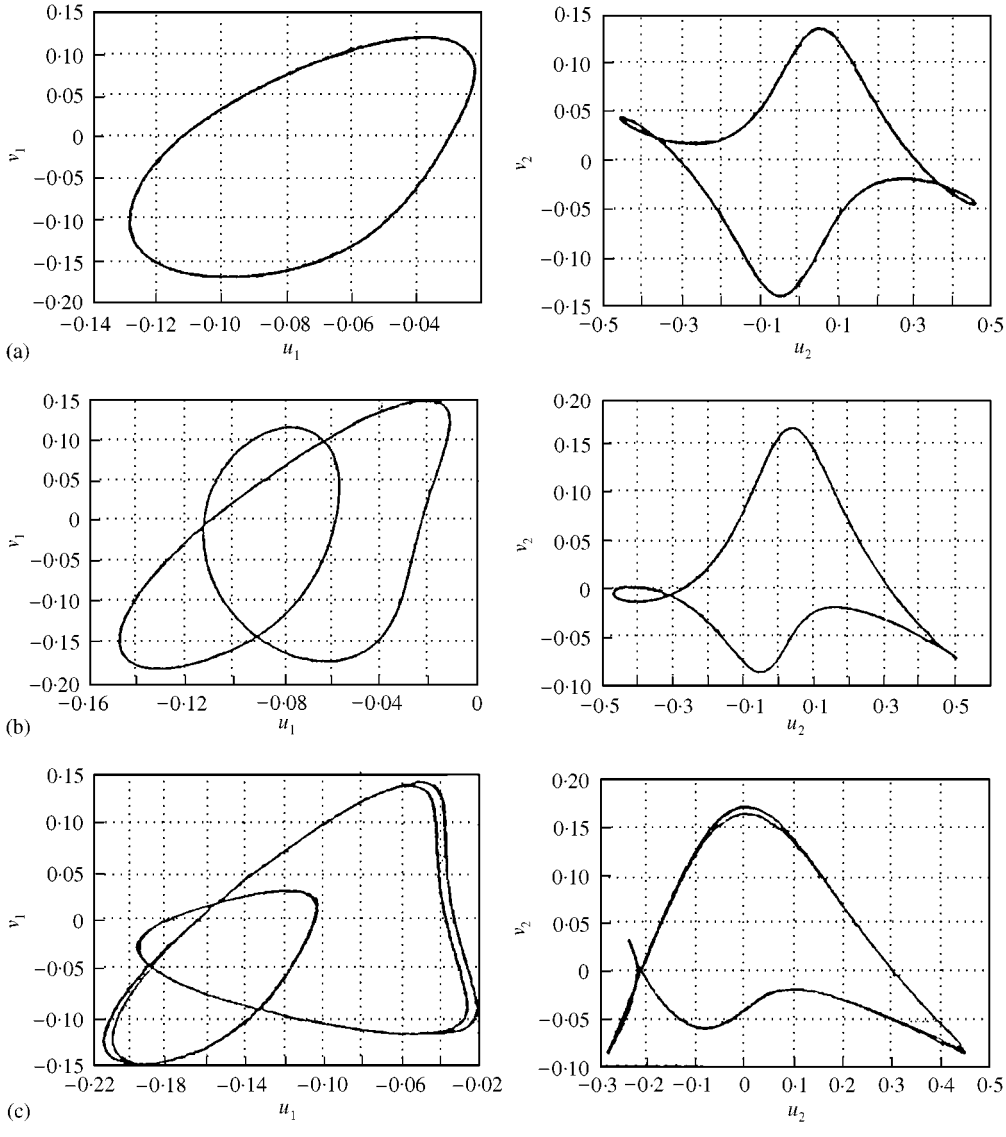

Figure 10. Period-doubling to chaos. (a) Period-1, (b) period-2, (c) period-4, (d) period-8, (e) chaos.

bifurcations, which is shown in Figure 10(a–e), where the bifurcation parameter—detuning parameter σ_1 is taken at $\sigma_1 = -1{\cdot}46$, $-1{\cdot}42$, $-1{\cdot}40$, $-1{\cdot}38$, $-1{\cdot}37$ respectively. The Poincare map—strange attractor at the cross-section $u_2 = 0$ is shown in Figure 11 when $\sigma_1 = -1{\cdot}25$.

When σ_1 is further increased to $-0{\cdot}07$, the chaos leads to modulated motion—Hopf bifurcation solution. The phase portraits of (u_1, v_1) and (u_2, v_2) are given in Figure 12(a–c), where the attractors in Figure 12(b, c) are symmetric to each other. The two attractors exist at the same time but correspond to different attracting basins.

In the chaos region, period-3 solution can be observed obviously. The portraits of period-6 for (u_1, v_1) and period-3 for (u_2, v_2) are shown in Figure 13(a, b) when $\sigma_1 = -1{\cdot}34$. Note that the symmetric attractors are omitted for simplicity.

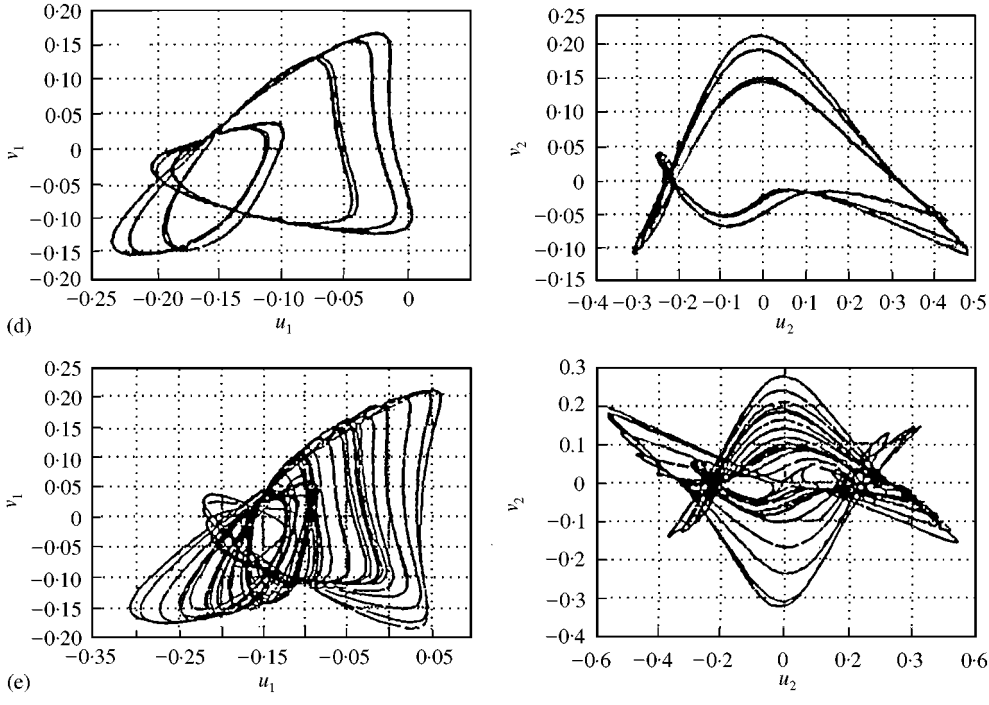

Figure 10. Continued.

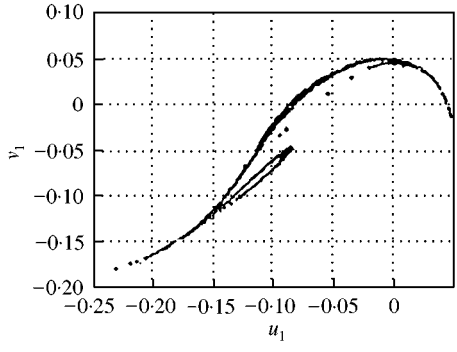

Figure 11. Poincare map at the cross-section $u_2 = 0$.

5. CONCLUSION

When the shallow arch is subjected to periodic excitation, the internal resonance occurs between the first order and the second order modes. The parametric plane can be divided into different types of regions according to the types of motions. The single-mode motion loses its stability and the coupled-mode motion occurs by simple bifurcation. The coupled-mode motion turns to modulated motion undergoing a Hopf bifurcation. The system leads to chaos via a sequence of period-doubling bifurcations. In the chaos region, a period-1 solution is found and it turns to chaos quickly by a set of period-doubling bifurcations. Period-3 is also found in the chaos region, which soon loses its stability.

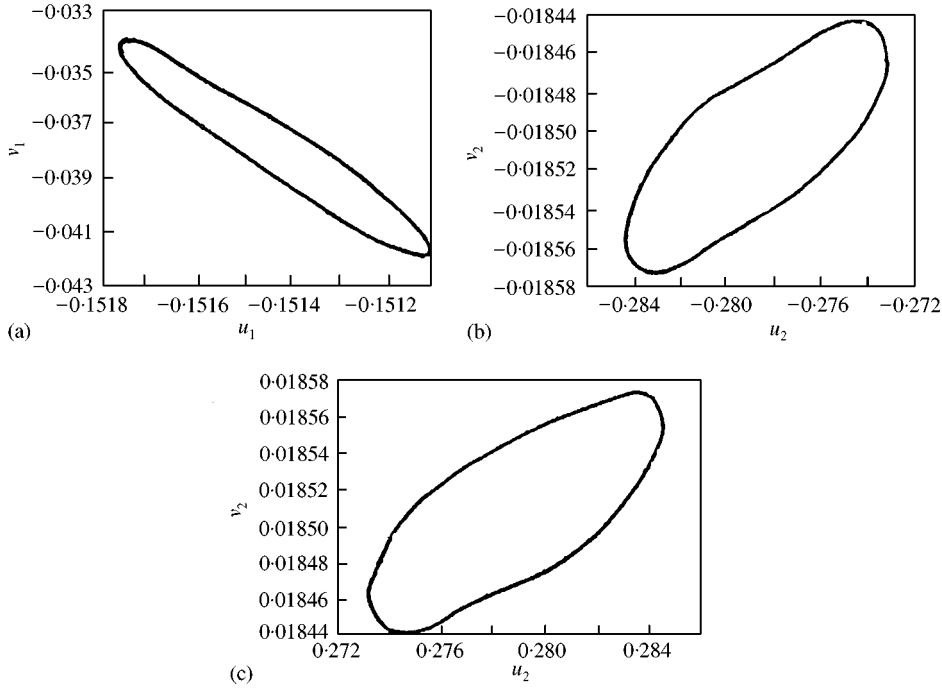

Figure 12. Hopf bifurcation solutions.

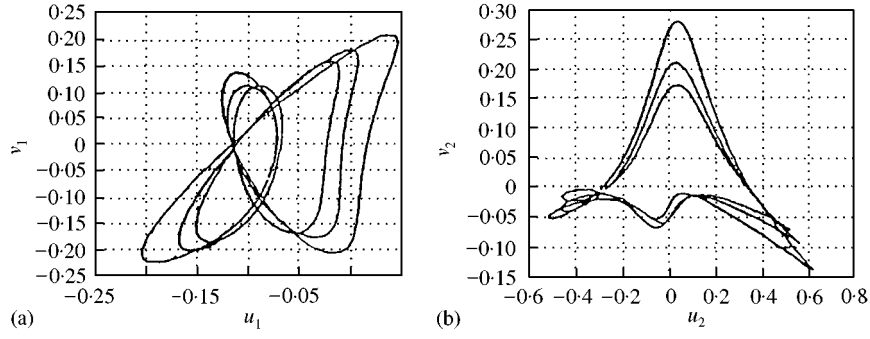

Figure 13. Period-6 solution for (u_1, v_1) and period-3 solution for (u_2, v_2).

ACKNOWLEDGMENTS

This work is supported by a CERG Grant (9040282) from Hong Kong Government and the National Natural Science Foundation of China (19902012).

REFERENCES

1. A. H. NAYFEH 1989 *Applied Mechanics Review* **42**, 175–201. Model interactions in dynamical and structural systems.
2. Z. C. FENG and P. R. SETHNA 1990 *Dynamics and Stability of Systems* **5**, 201–225. Global bifurcation and chaos in parametrically forced system with one–one resonance.

3. A. BAJAJ and P. R. SETHNA 1984 *Journal of Applied Mathematics* **44**, 270–286. Flow induced vibrations to three-dimensional oscillatory motions in continuous tubes.
4. J. W. MILES 1984 *Journal of Acoustics Society of America* **15**, 1505–1510. Resonant, non-planar motion of a stretched string.
5. L. K. JOHNSON and A. K. BAJAJ 1989 *Journal of Sound and Vibration* **155**, 87–107. Amplitude modulated and chaotic dynamics in resonant motion in strings.
6. P. YU and Q. BI 1998 *Journal of Sound and Vibration* **217**, 691–736. Analysis of non-linear dynamics and bifurcations of a double pendulum.
7. W.-M. TIEN, N. SRI NAMACHCHIVAYA and A. K. BAJAJ 1994 *International Journal of Non-linear Mechanics* **29**, 349–366. Non-linear dynamics of a shallow arch under periodic excitation—II. 1 : 2 internal resonance.
8. W.-M. TIEN, N. SRI NAMACHCHIVAYA and A. K. BAJAJ 1994 *International Journal of Non-linear Mechanics* **29**, 367–386. Non-linear dynamics of a shallow arch under periodic excitation—I. 1 : 1 internal resonance.
9. G. KOVACIC and S. WIGGINS 1992 *Physica D* **57**, 185–225. Orbits homoclinic to resonances with an application to chaos in a model of the forced and damped Sine–Gordon equation.